Journal of Materials Chemistry A

Accepted Manuscript

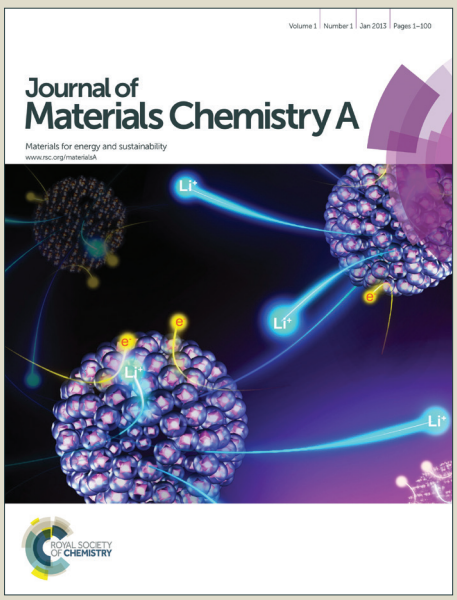

ROYAL SOCIETY OF CHEMISTRY

www.rsc.org/materialsA

Journal Name RSCPublishing

ARTICLE

Three-dimensional porous graphene/polyaniline composites for high-rate electrochemical capacitors

Cite this: DOI: 10.1039/x0xx00000x

Qinqin Zhou, Yingru Li, Liang Huang, Chun Li, Gaoquan Shi*

Received 00th January 2012,
Accepted 00th January 2012

DOI: 10.1039/x0xx00000x

www.rsc.org/

We report an electrochemical co-deposition method to prepare three-dimensional (3D) porous composites of reduced graphene oxide (rGO) and polyaniline (PANI) with pores vertically oriented on the surfaces of current collectors and used as an electrode material of electrochemical capacitors (ECs). These composites showed much larger areal specific capacitances and greatly improved rate capability than those of PANI. Typically, the rGO/PANI composite film with a thickness of 150 μm exhibited a high areal specific capacitance (C_a, 67.2 mF cm^{-2}), small relaxation time constant (τ_0, 316 ms) and good electrochemical stability, promising for the fabrication of high-rate EC.

Introduction

Electrochemical capacitors (ECs) are attractive energy storage devices because of their high power densities, fast charge-discharge processes and long cycling life.[1–3] According to their energy storage mechanisms, ECs are classified as electronic double layer capacitors (EDLCs) and pseudocapacitors.[3] The former accumulates charges at the interfaces of electrodes and electrolytes, and the latter stores energy by reversible redox reactions of electrode materials. Polyaniline (PANI) has been extensively studied among conductive polymers for pseudocapacitors mainly due to its high specific pseudocapacitance, ease of synthesis, good environmental stability, and low cost.[4–6] However, the cycling life and rate-capability of PANI electrodes are unsatisfactory because of their large volume changes, slow redox reactions during charging/discharging processes.[7,8] Furthermore, the low conductivity of neutral PANI also weakens its performances in ECs. To address these problems, PANI was frequently blended with carbon nanomaterials to improve its conductivity, mechanical and electrochemical stabilities and the kinetics of redox reactions.[9–11]

Among carbon nanomaterials,[12–15] graphene is unique and attractive because of its huge specific surface area, high conductivity, and good electrochemical and mechanical stabilities.[16,17] Recently, graphene/PANI composites have been prepared by in-situ chemical oxidative polymerization,[18–20] electropolymerization[5,21–23] or interfacial polymerization[24–26] for the fabrication of ECs. Chemical oxidative polymerization usually produces a powdery composite. Interfacial polymerization involves using a toxic organic solvent, and the morphology of product is difficult to be controlled. On the other hand, electropolymerization has several advantages including short reaction time, oxidant-free, and the composites are directly deposited on the surfaces of current collectors, avoiding using binders and conductive fillers.[6,27,28] Nevertheless, the ECs based on electrodeposited PANI composites reported previously usually have unsatisfactory rate-performances because of their relatively compact morphology and heavily stacking of graphene sheets.[8,22,23]

High-rate ECs are important for the applications in AC-line filtering, aircrafts, automotive vehicles and power suppliers.[28] For these purposes, a variety of high-rate ECs were reported, while their areal specific capacitances are relatively low.[29,30] Herein, we report three-dimensional porous graphene/PANI composites with pores vertically oriented on current collector by one-step electrodeposition from the homogeneous mixed solution of aniline monomer and graphene oxide. In this case, graphene network provided not only a scaffold with large specific surface area for the deposition of PANI, but also highly conductive porous channels for the transfer of electrons and the facile adsorption-desorption of ions in electrolyte. Thus, the ECs based on these graphene/PANI composites exhibited much higher areal specific capacitances, excellent rate capability and improved cycling stability compared with those of the counterparts based on pristine PANI films.

Experimental section

Synthesis of graphene oxide (GO). GO was synthesized by the oxidation of natural graphite power (325 mesh, Qingdao Huatai Lubricant Sealing Science and Technology Co. Ltd., Qingdao, China) following a modified Hummers' method.[31, 32] It was purified by dialysis for a week to remove the remaining salts and acid impurities and centrifuged for 30 min at 4000 rpm to remove aggregates. Finally, the resulted GO dispersion was adjusted to 4.5 mg mL^{-1} for use.

Preparation of graphene/PANI composites. 68.5 μL distilled aniline was added to 5 mL twice distilled water. Then, this system was purged with nitrogen gas and sonicated at 20 °C for 10 min to form a transparent solution (solution A). 720 mg $LiClO_4 \bullet 3H_2O$ was dissolved in 10 mL GO dispersion (4.5 mg mL^{-1}) and sonicated for several minutes (solution B). Successively, solutions A and B were mixed by sonication for 10 min under a deoxygenated condition, and the resulting mixture was used as the electrolyte for electrosynthesis. The electrochemical co-deposition was carried out in a dark environment using cyclic voltammetry at a scan rate of 50 mV s^{-1} in a potential range of −1.2 V to 0.8 V. Gold (Au) and platinum (Pt) foils were used as the working and the counter electrodes, respectively, and the potentials were referred to a saturated calomel electrode (SCE). For control experiments, PANI films were synthesized *via* cyclic voltammetry scanning in the potential range of 0–0.8 V at 50 mV s^{-1}. Pure rGO films were also grown by cyclic voltammetry scanning in the potential range of −1.2 to 0 V at 50 mV s^{-1}. These samples were washed repeatedly with water to remove the absorbed monomer and/or the residual salts. They were immersed in 1 M H_2SO_4 electrolyte before electrochemical tests.

The rGO, PANI and Graphene/PANI composites were prepared by cyclic voltammetry scanning for different cycles, and they were nominated as rGO_n, $PANI_n$, and GP_n, respectively (n is the number of CV cycles).

Electrochemical measurements. Cyclic voltammograms (CV), electrochemical impedance spectra (EIS) and galvanostatic charge–discharge tests were performed by the use of a CHI 660B Potentiostat (CH Instruments, Inc.). The Au electrode coated with electrode material was used as the working electrode. The counter electrode was a Pt foil and the reference electrode was a SCE. EIS spectra were recorded in the frequency range of 0.01 to 10^5 Hz with a 5 mV amplitude referring to the open circuit potential. It should be noted here that the electrode material (e.g. rGO_n, $PANI_n$ or GP_n) is too light to be weighted accurately as n is smaller than 10. Thus, the specific capacitances of EC electrodes were evaluated in area units (mF cm^{-2}). The areal specific capacitance (C_a) was calculated by the equation $C_a = I\Delta t/s\Delta V$, where I is the constant discharge current, Δt is the discharge time, ΔV is the discharge potential drop (excluding IR drop), and s is the area of electrode.

The performances of rGO_{100}, GP_{20} and $PANI_{100}$ have also been examined in a two-electrode system. This is mainly due to that the loadings of GP_{20} and $PANI_{100}$ electrodes were measured to be nearly the same (0.17 ± 0.03 mg cm^{-2}). CVs were carried out in a potential range of −0.2 to 0.8 V and galvanostatic charge–discharge tests were performed in the potential range of 0 to 0.8 V. In this case, C_a was calculated by $C_a = 2I\Delta t/s\Delta V$.

Characterizations. The morphologies of electrode materials were studied by using a field-emission scanning electron microscope (SEM, Sirion200) and a FEI TECNAI TF20 transmission electron microscope (TEM). Raman spectra were recorded on a LabRAM HR Evolution Raman spectrometer (Horiba Jobin Yvon) with a 514-nm laser. X-ray photoelectron spectroscopic (XPS) examinations were carried out by using an ESCALAB 250 photoelectron spectrometer (ThermoFisher Scientific, USA).

Results and discussion

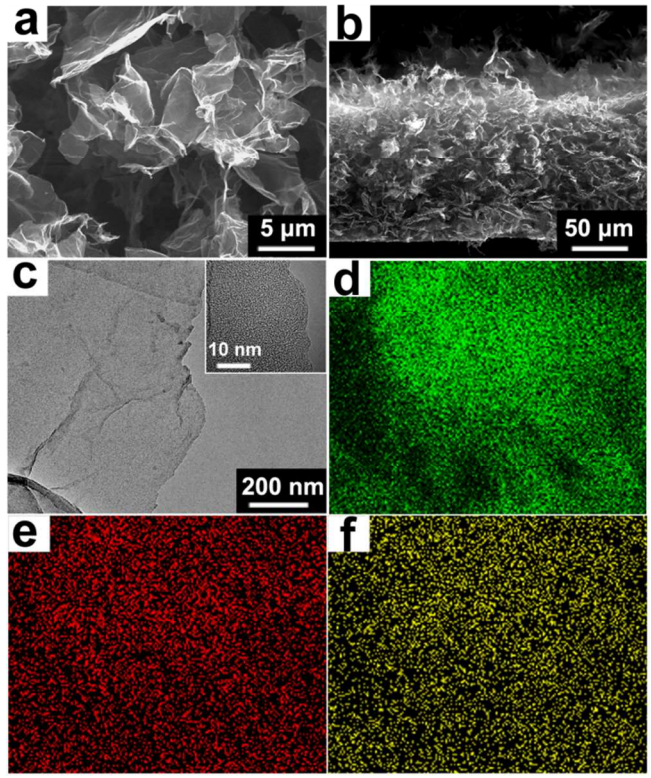

Fig. 1 (a)Top view and (b) cross-section SEM images, and (c) TEM image of GP_{20} (inset: HR-TEM image); (d-e) The element mapping images of carbon (d), nitrogen (e) and oxygen (f) for the marked region in panel (a).

The graphene/PANI composites were prepared by one-step cyclic voltammetry scanning in the potential range of −1.2 to 0.8 V. The initial potential was controlled to be −1.2 V; thus, GO sheets were firstly electrochemically reduced to form a rGO layer on the substrate electrode, and then aniline monomers were oxidized and polymerized on the surfaces of rGO sheets at the positive potentials.[5, 22] The composites grown for different CV cycles have similar morphologies, while their microstructures were slightly changed to be more irregular and compact with the increasing in CV cycling number. Meanwhile, the thickness of the composite layer increased nearly linearly with the increase in the number of CV cycles (GP1 ~31 μm, GP3 ~52 μm, GP6 ~72 μm, GP10 ~107 μm, Fig. S1†). Here, GP_{20} (e. g. the composite grown for 20 CV cycles) is taken as an example. GP_{20} has a 3D porous microstructure (Fig. 1a) with a thickness of about 150 μm (Fig. 1b). In comparison, the pure PANI film deposited under the same condition is a granular film (Fig. S2†). The composite sheets of GP_{20} (Fig. 1c) are thicker and more blurred than pure rGO sheets (Fig. S3†), indicating the coating of PANI on the surfaces of rGO sheets.

The HR-TEM image of a GP20 sheet (inset of Fig. 1c) also confirms this conclusion. The element mapping images (for the

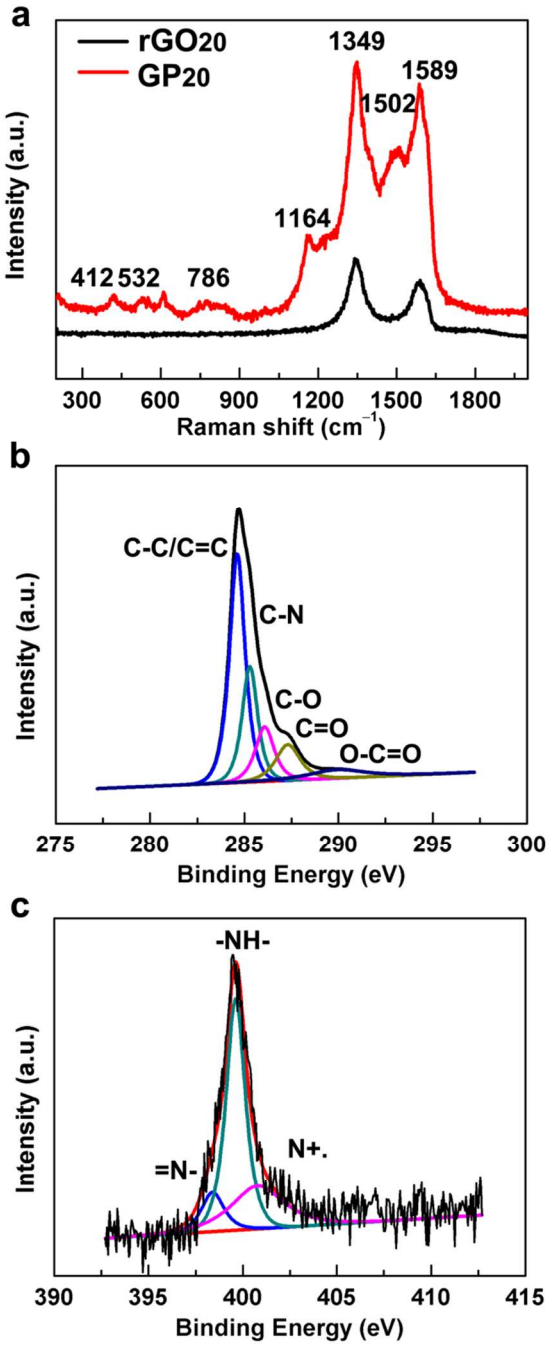

Fig. 2 (a) Raman spectra of rGO_{20} and GP_{20}; (b, c) C 1s (b) and N 1s (c) XPS spectra of GP_{20}.

marked region of Fig. 1a) demonstrate the homogeneous distributions of carbon, nitrogen and oxygen elements in GP_{20} (Fig. 1d to 1f), reflecting the formation of a uniform rGO/PANI composite. As described above, PANI layer coated on the surface of conductive rGO framework with hierarchical pores fully exposed to the electrolyte for the access of ions to form electrochemical double layers and supporting the redox reactions of PANI.

Fig. 2a illustrates the Raman spectra of rGO_{20} and GP_{20}. The spectrum of rGO_{20} has two dominant peaks at 1346 and

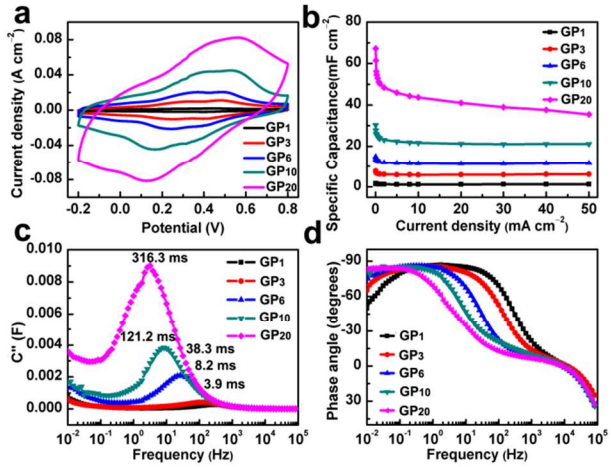

Fig. 3 (a) CV curves of GP_n electrodes at a scan rate of 1 V s^{-1}; (b) Plots of areal specific capacitances of GP_n electrodes versus discharge current densities; (c, d) Bode plots of the imaginary areal specific capacitances (c) or phase angles (d) versus frequencies.

1586 cm^{-1}, corresponding to its D and G bands.[33,34] In the spectrum of GP_{20}, the characteristic rGO bands slightly shifted to higher frequencies (1349 and 1589 cm^{-1}), possibly due to the interaction between rGO sheets and PANI chains. This spectrum also shows the characteristic Raman bands of PANI. The Raman band at 421 cm^{-1} is associated with the out-of-plane C–H wag. The band related to phenazine-like segment appears at around 532 cm^{-1}. The 786 cm^{-1} band is assigned to the imine deformation. The 1164 and 1502 cm^{-1} bands are associated with the in-plane C–H bending and C=N stretching vibrations of the quinonoid units.[18, 21]

The C 1s XPS spectrum of GP_{20} demonstrates five types of carbon bonds: C-C/C=C (284.6 eV), C-N (285.3 eV), C-O (286.1 eV), C=O (287.3 eV) and O-C=O (289.9 eV) (Fig. 2b).[5,23] The relative intensities of oxygen functionalities in this spectrum are much weaker than those of GO (Fig. S4†). Actually, the C/O atomic ratio of rGO component in GP_{20} composite was calculated to be 3.03. This value is higher than that of GO (2.26), confirming that the GO sheets have been partially reduced. The N 1s XPS spectrum of GP_{20} shows three peaks located at 398.4, 399.6, and 400.8 eV, and they are assigned to benzenoid amine (=N-), quinoid amine (-NH-) and nitrogen cationic radical ($N^{+\cdot}$), respectively (Fig. 2c). The Raman and XPS spectra results described above also confirm the successful growth of graphene/PANI composites.[5,35]

The electrochemical capacitive performances of the graphene/PANI composites were studied by CVs, charge-discharge tests and EIS spectra. Each CV curve of the composites has a quasi-rectangular shaped baseline current and two pairs of redox waves at a high scan rate of 1 V s^{-1} (Fig. 3a, Fig. S5a†). The baseline current is attributed to the electrochemical double layers capacitance of the electrode and the redox waves are associated with the

leucoemeraldine/emeraldine and emeraldine/pernigraniline transformations of PANI, correspondingly.[36,37] These two-couples of redox peaks of PANI can be observed from the CV curves at ultra-fast scan rates: up to 50 V s^{-1} for GP_1, 10 V s^{-1} for GP_3, 5 V s^{-1} for GP_6, 2 V s^{-1} for GP_{10} and 1 V s^{-1} for GP_{20} (Fig. S5b-f†). In comparison, a PANI film grown for 20 CV cycles shows a C_a comparable to that of GP_1. However, its CV is severely distorted from the curve with two-couples of redox waves at 5 V s^{-1}, reflecting its much worse rate capability than that of GP_1 (Fig. S6†). The C_as of GP_1, GP_3, GP_6, GP_{10} and GP_{20} were measured to be 1.6, 7.7, 14.9, 30.3 and 67.2 mF cm^{-2}, respectively, at a discharge current density (i_d) of 50 μA cm^{-2}. In addition, the capacitance retention was tested to be 99.5 % for GP_1, 96.1% for GP_3, 92.7 % for GP_6, 85.4 % for GP_{10} and 67.0 % for GP_{20} as i_d increased from 0.5 to 50 mA cm^{-2} (Fig 3b). These results reflect the 3D porous GP_n electrodes have excellent rate capability. Moreover, GP_1, GP_3, GP_6, GP_{10} and GP_{20} still remain C_as of 1.3, 6.1, 11.6, 21.1 and 35.4 mF cm^{-2} at an i_d = 50 mA cm^{-2}, respectively. Accordingly, these electrodes can be operated at several tens to several hundreds ms level (Fig. S7†), comparable to the most rapid counterparts based on graphene or graphene composites.[7, 17, 38, 39] Furthermore, the C_as of the GP_n ($n \geqslant 3$) composites are twice to over ten times higher than those of the high-rate carbon electrodes such as onion-like carbon (1.7 mF cm^{-2} at a potential scan rate of 1 V s^{-1}),[29] activated carbon (4.5 mF cm^{-2})[29] and laser scribed graphene film (3.67 mF cm^{-2} at i_d = 36.3 μA cm^{-2}).[30] This is mainly attributed to the combined contributions of graphene electrochemical double layers capacitance and PANI faradic capacitance in the 3D porous composites.

Relaxation time constant (τ_0) is another parameter to evaluate the rate capability of capacitive electrodes.[40] The reciprocal of the frequency at which the imaginary specific capacitance reaches the maximum is τ_0.[41] The τ_0s of GP_1, GP_3, GP_6, GP_{10} and GP_{20} were tested to be 3.9 ms (258.8 Hz), 8.2 ms (122.1 Hz), 38.3 ms (26.1 Hz), 121.2 ms (8.254 Hz) and 316.3 ms (3.162 Hz), respectively (Fig. 3c). The τ_0s of GP_1 and GP_3 are shorter than those of reported onion-like carbon (26 ms)[29], activated carbon (700 ms)[29] and multilayered graphene (13.3 ms)[42] based high-rate EDLCs. Fig. 3d shows that the phase angle of each electrode increases up to around 90 degrees with the decreasing of frequency and shows a platform at low frequencies. In the region of platform, PANI can be nearly fully used to contribute capacitance.[43] The highest frequency of the plateaus for GP_1 was measured to be about 38 Hz, and this value is much higher than that of other GP_n electrodes (12.12 Hz for GP_3, 3.162 Hz for GP_6, 1.468 Hz for GP_{10} and 0.3162 Hz for GP_{20}), indicating its best rate-performance. These results reflect the fast transports of electrons and ions in the composite electrodes. In the composites, the porous graphene framework provided a highly conductive support for PANI, shortening the charge transfer distance from PANI to current collector.[44] In addition, the 3D architecture with hierarchical pores oriented vertically to the surface of current collector, providing a large specific area accessible to electrolyte.

The electrochemical capacitive performances of graphene/PANI composites were compared with those of their single components. We chose GP_{20}, rGO_{100} and $PANI_{100}$ as examples because they have comparable C_as (Fig. S8†). The

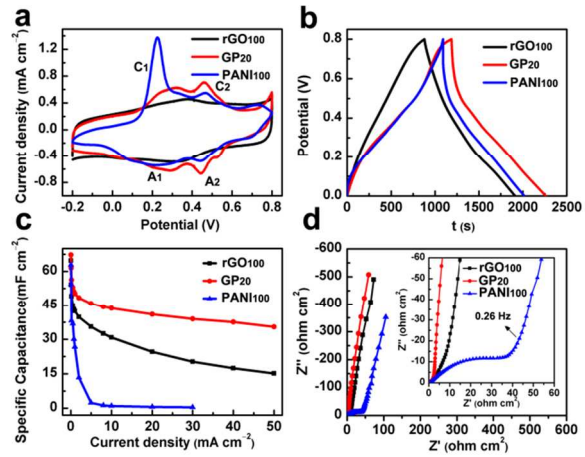

Fig. 4 (a) CVs of rGO_{100}, GP_{20} and $PANI_{100}$ electrodes at a scan rate of 5 mV s^{-1}; (b) galvanostatic charge–discharge curves of rGO_{100}, GP_{20} and $PANI_{100}$ electrodes at an i_d of 50 μA cm^{-2}; (c) Areal specific capacitances calculated from the charge-discharge curves of rGO_{100}, GP_{20} and $PANI_{100}$ electrodes at different i_ds; (d) Nyquist plots of rGO_{100}, GP_{20} and $PANI_{100}$ electrodes.

large quasi-rectangular areas of all CV curves at 5 mV s^{-1} are attributed to electrochemical double-layer (EDL) capacitances (Fig. 4a). The CV curve of GP_{20} or $PANI_{100}$ exhibits two-couples of redox peaks (C_1 ~ 0.22 V, A_1~ 0.22 V; C_2 ~ 0.46 V, A_2 ~ 0.44 V). The C_1 peak of GP_{20} is broader than that of $PANI_{100}$, possibly due to the presence of redox reaction of residual oxygenated groups of rGO sheets. As the scan rate increased to 100 mV s^{-1}, the CV curves of rGO_{100} and GP_{20} kept their primitive shapes, while that of PANI was severely distorted (Fig. S9a†). The charge-discharge curves of rGO_{100}, GP_{20} and $PANI_{100}$ at i_d = 50 μA cm^{-2} are demonstrated in Fig. 4b. The curve of rGO_{100} has a nearly symmetric triangle shape, indicating a dominant EDL capacitance. However, the curves of GP_{20} has a nonlinear shape with two sections. The first section in the potential range of 0.8–0.45 V has a short discharge duration, and it is associated with EDL capacitance and the second section ranging from 0 to 0.45 V is related to a combination of EDL and redox capacitances from PANI.[4, 5] The discharge curve of $PANI_{100}$ has a shape similar to that of GP_{20}. However, $PANI_{100}$ electrode showed a much larger "IR drop" (0.39 V) than that of GP_{20} electrode (0.037 V) at the same i_d = 10 mA cm^{-2} (Fig. S9b†). This result implies $PANI_{100}$ film has a larger internal resistance, which waste more energy to produce unwanted heat. Therefore, GP_{20} is more suitable for power-saving device compared with $PANI_{100}$.

The C_as of rGO_{100}, GP_{20} and $PANI_{100}$ measured by charging-discharging tests are plotted in Fig. 4c. The C_as of rGO_{100}, GP_{20} and $PANI_{100}$ were measured to be 64.7, 67.2 and 62.9 mF cm^{-2} at i_d =50 μA cm^{-2}, respectively. However, GP_{20} kept about 82.5 % of initial capacitance as i_d increased from 0.5 to 10 mA cm^{-2}, while the capacitance retentions of rGO_{100} and $PANI_{100}$ were

found to be only 68.5 % and 2.7 % in the same i_d range. At i_d = 10 mA cm^{-2}, the C_a of GP_{20} (43.7 mF cm^{-2}) is more than 40 times that of $PANI_{100}$ (1.0 mF cm^{-2}). Furthermore, GP_{20} kept a C_a of 35.4 mF cm^{-2} as i_d increased to 50 mA cm^{-2}, indicating it has the best rate capability.

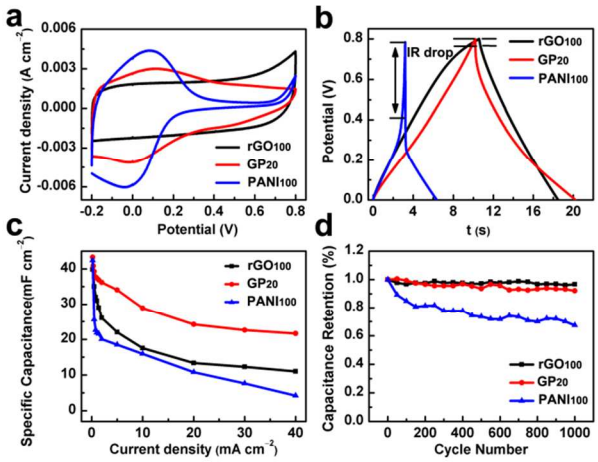

Fig. 5 (a) CV curves of rGO_{100}, GP_{20} and $PANI_{100}$ based ECs at a scan rate of 100 mV s^{-1}; (b) Galvanostatic charge–discharge curves of rGO_{100}, GP_{20} and $PANI_{100}$ based ECs at an i_d of 1.4 mA cm^{-2}; (c) Areal specific capacitances calculated from charge-discharge curves of GP_{20} and $PANI_{100}$ based ECs in a large range of current densities; (d) Cycling stability of GP_{20} and $PANI_{100}$ based ECs at an i_d of 1.4 mA cm^{-2}. All the experiments were performed in two-electrode systems.

EIS is an effective method to measure the internal resistances and charge transfer kinetics of electrodes.[45] The Nyquist plots of rGO_{100}, GP_{20} and $PANI_{100}$ electrodes are shown in Fig. 4d. In general, a Nyquist plot composes of a semicircle in high frequency region associated with charge transfer resistance (R_{ct}), 45° section in middle frequency region corresponding to porous structure of the electrode and a straight line in low frequency region related to capacitive behaviour. According to the magnified plots (inset of Fig. 4d, Fig. S9c†), the equivalent series resistances (ESR) were measured to be 1.7 Ω for rGO_{100}, 1.1 Ω for GP_{20} and 38.8 Ω for $PANI_{100}$ by extrapolating the straight line to intersect Z' axes.[46] The ESR is assigned to electrolyte solution resistance, intrinsic resistance of active materials and the interfacial contact resistance between active materials and current collector.[43] Furthermore, R_{ct} of $PANI_{100}$ electrode (34.3 Ω), corresponding to the diameter of incomplete semicircle, is much larger than that of rGO_{100} (0.22 Ω) and GP_{20} (a inconspicuous loop) electrodes, demonstrating the incorporation of 3D rGO framework improved the conductivity of GP_{20}. The transition point between 45° region and the vertical line in the low-frequency is generally called "knee" frequency. It is the maximum frequency at which the capacitive behaviour is dominant.[47] The "knee" frequencies of rGO_{100}, GP_{20} and $PANI_{100}$ are 6.81, 21.54 and 0.26 Hz, respectively, implying GP_{20} electrodes exhibits a capacitive behaviour at the highest frequency compared with those of rGO_{100} and $PANI_{100}$. Furthermore, the slope of the low-frequency region for GP_{20} electrode is larger than those of rGO_{100} and $PANI_{100}$, suggesting a faster ion diffusion of electrolyte. These results further demonstrate that GP_{20} electrode has much higher conductivity and a better ion diffusion behaviour than those of rGO_{100} and $PANI_{100}$, leading to its excellent rate capability. Furthermore, the τ_0 of GP_{20} electrode (316.3 ms) is much shorter than that of rGO_{100} (2.61 s) and $PANI_{100}$ (17.8 s) (Fig. S9d†), also reflecting its best rate capability. However, as the τ_0s of electrodes were controlled to be the same (τ_0=316.3 ms), GP_{20} possesses the largest C_a (67.2 mF cm^{-2}) compared with those of rGO_{21} (18.8 mF cm^{-2}) and $PANI_5$ (0.8 mF cm^{-2}) (Fig. S10†). On the basis of the results described above, it is reasonable to conclude that GP_{20} electrode has a large areal specific capacitance and an excellent rate-performance.

The electrochemical performances of rGO_{100}, GP_{20} and $PANI_{100}$ were also evaluated in a more practical two-electrode system. The CV curve of GP_{20} exhibits a characteristic shape combined with EDL and redox capacitances (Fig. 5a). Meanwhile, the discharge curve of the EC based on GP_{20} shows a much smaller "IR drop" than that of the EC based on $PANI_{100}$, implying an enhanced conductivity of the GP_{20} electrodes (Fig. 5b). The C_a of GP_{20} based EC was measured to be about 43.3 mF cm^{-2} at an i_d of 0.2 mA cm^{-2} (Fig. 5c). As i_d increased from 0.2 to 40 mA cm^{-2}, the capacitance retention of GP_{20} based EC (50.0%) is much higher than those of rGO_{100} (29.1%) and $PANI_{100}$ (10.0%) based ECs, exhibiting the similar characteristic as that measured in the three-electrode systems described above. The most serious problem of PANI-based ECs is their poor cycling stability caused by the volume changes of electrode material during the process of doping-dedoping process. As is shown in Fig. 5d, the GP_{20} based EC exhibits a good stability with a capacitance retention of 92 % after 1000 cycles of charge-discharge tests at i_d = 1.4 mA cm^{-2}, which is comparable to that of rGO_{100} based EC. In comparison, under the same condition, the capacitance retention of pristine PANI based EC was measured to be only 67%. Furthermore, the durability of GP_{20} based EC is much better than that of the EC based on graphene/PANI fibre composites (79%, at 3 A g^{-1})[4] or PANI electrodeposited on graphene paper (82%, at 5 A g^{-1}).[48] The improved stability performance of GP_{20} based EC is mainly due to the graphene sheets provide a flexible, mechanically strong and electrically conductive network to accommodate the volume changes of PANI, delivering electrons efficiently to the current collectors.

Conclusions

3D porous rGO/PANI composites were successfully prepared by electrochemical co-deposition. Graphene component provides a porous conductive support with large specific surface for PANI, improving the efficiency of using PANI and facilitating ion or charge transfer in the electrodes. These composites can be directly used as electrode materials of ECs, without using binder and conductive filler. The ECs based on GP composites have high areal specific capacitances, and good electrochemical stability. Particularly, they exhibited excellent rate-capability, promising to deliver large power within a short time.

Acknowledgements

This work was supported by the National Basic Research Program of China (973 Program, 2012CB933402) and the Natural Science Foundation of China (51161120361, 21274074).

Notes and references

Department of Chemistry, Tsinghua University, Beijing 100084, People's Republic of China. Fax: 86 62771149; Tel: 86 6277 3743; E-mail: gshi@tsinghua.edu.cn

† Electronic Supplementary Information (ESI) available: [Supplementary figures about the morphologies, structures and electrochemical performances of different electrode materials]. See DOI: 10.1039/b000000x/

1 P. Simon and Y. Gogotsi, *Nat. Mater.*, 2008, **7**, 845–854.
2 J. R. Miller and P. Simon, *Science*, 2008, **321**, 651–652.
3 H. Jiang, P. S. Lee and C. Z. Li, *Energy Environ. Sci.*, 2013, **6**, 41–53.
4 Q. Wu, Y. X. Xu, Z. Y. Yao, A. R. Liu and G. Q. Shi, *ACS Nano*, 2010, **4**, 1963–1970.
5 X. M. Feng, R. M. Li, Y. W. Ma, R. F. Chen, N. E. Shi, Q. L. Fan and W. Huang, *Adv. Funct. Mater.*, 2011, **21**, 2989–2996.
6 L. Wang, X. P. Lu, S. B. Lei and Y. H. Song, *J. Mater. Chem. A*, 2014, **2**, 4491–4509.
7 Y. F. Wang, X. W. Yang, L. Qiu and D. Li, *Energy Environ. Sci.*, 2013, **6**, 477–481.
8 Q. Q. Zhang, Y. Li, Y. Y. Feng and W. Feng, *Electrochim. Acta*, 2013, **90**, 95–100.
9 J. Yan, T. Wei, Z. J. Fan, W. Z. Qian, M. L. Zhang, X. D. Shen and F. Wei, *J. Power Sources*, 2010, **195**, 3041–3045.
10 G. H. Yu, X. Xie, L. J. Pan, Z. N. Bao and Y. Cui, *Nano Energy*, 2013, **2**, 213–234.
11 N. A. Kumar and J. B. Baek, *Chem. Commun.*, 2014, **50**, 6298–6300.
12. X. J. He, N. Zhao, J. S. Qiu, N. Xiao, M. X. Yu, C. Yu, X. Y.Zhang and M. D. Zheng, *J. Mater. Chem. A*, 2013, **1**, 9440–9448.
13. X. J. He, P. H. Ling, J. S. Qiu, M. X. Yu, X. Y. Zhang, C. Yu and M. D. Zheng, *J. Power Sources*, 2013, **240**, 109–113.
14. Z. Y. Cao and B. Q. Wei, *Energy Environ. Sci.*, 2013, **6**, 3183–3201.
15. Y. Zhou, N. Lachman, M. Ghaffari, H. P. Xu, D. Bhattacharya, P. Fattahi, M. R. Abidian, S. Wu, K. K. Gleason, B. L. Wardle and Q. M. Zhang, *J. Mater. Chem. A*, 2014, **2**, 9964–9969.
16 M. D. Stoller, S. Park, Y. Zhu, J. An and R. S. Ruoff, *Nano Lett.*, 2008, **8**, 3498–3502.
17 J. Chen, K. X. Sheng, P. H. Luo, C. Li and G. Q. Shi, *Adv. Mater.*, 2012, **24**, 4569–4573.
18 H. L. Wang, Q. L. Hao, X. J. Yang, L. D. Lu and X. Wang, *Nanoscale*, 2010, **2**, 2164–2170.
19 J. J. Xu, K. Wang, S. Z. Zu, B. H. Han and Z. X. Wei, *ACS Nano*, 2010, **4**, 5019–5026.
20 N. A. Kumar, H. J. Choi, Y. R. Shin, D. W. Chang, L. M. Dai and J. B. Baek, *ACS Nano*, 2012, **6**, 1715–1723.
21 Y. Zhao, H. Bai, Y. Hu, Y. Li, L. T. Qu, S. W. Zhang and G. Q. Shi, *J. Mater. Chem.*, 2011, **21**, 13978–13983.
22 X. Q. Jiang, S. Setodoi, S. Fukumoto, I. Imae, K. Komaguchi, J. Yano, H. Mizota and Y. Harima, *Carbon*, 2014, **67**, 662–672.
23 T. Lindfors and R. M. Latonen, *Carbon*, 2014, **69**, 122–131.
24 J. H. Zhu, M. J. Chen, H. L. Qu, X. Zhang, H. G. Wei, Z. P. Luo, H. A. Colorado, S. Y. Wei and Z. H. Guo, *Polymer*, 2012, **53**, 5953–5964.
25 B. Ma, X. Zhou, H. Bao, X. W. Li and G. C. Wang, *J. Power Sources*, 2012, **215**, 36–42.
26 J. L. Shen, C. Y. Yang, X.W. Li and G. C. Wang, *ACS Appl. Mater. Interfaces*, 2013, **5**, 8467–8476.
27 C. Peng, J. Jin 25and G. Z. Chen, *Electrochim. Acta*, 2007, **53**, 525–537.
28 J. Chen, C. Li and G. Q. Shi, *J. Phys. Chem. Lett.*, 2013, **4**, 1244–1253.
29 D. Pech, M. Brunet, H. Durou, P. H. Huang, V. Mochalin, Y. Gogotsi, P. L. Taberna and P. Simon, *Nat. Nanotechnol.*, 2010, **5**, 651–654.
30 M. F. El-Kady, V. Strong, S. Dubin and R. B. Kaner, *Science*, 2012, **335**, 1326–1330.
31 W. S. Hummers, R. E. Offeman, *J. Am. Chem.Soc*, 1958, **80**, 1339–1339.
32 Y. X. Xu, K. X. Sheng, C. Li and G. Q. Shi, *ACS Nano*, 2010, **4**, 4324–4330.
33 K. X. Sheng, Y. Q. Sun, C. Li, W. J. Yuan and G. Q. Shi, *Sci. Rep.*, 2012, **2,** 247.
34 Y. R. Li, K. X. Sheng, W. J. Yuan and G. Q. Shi, *Chem. Commun.*, 2013, **49**, 291–293.
35 T. Lee, T. Yun, B. Park, B. Sharma, H. K. Song and B. S. Kim, *J. Mater. Chem.*, 2012, **22**, 21092–21099.
36 S. J. He, X. W. Hu, S. L. Chen, H. Hu, M. Hanif and H. Q. Hou, *J. Mater. Chem.*, 2012, **22**, 5114–5120.
37 Y. F. Xu, M. G. Schwab, A. J. Strudwick, I. Hennig, X. L. Feng, Z. S. Wu and K. Müllen, *Adv. Energy Mater.*, 2013, **3**, 1035–1040.
38 L. Zhang and G. Q. Shi, *J. Phys. Chem. C*, 2011, **115**, 17206–17212.
39 Y. N. Meng, K. Wang, Y. J. Zhang and Z. X. Wei, *Adv. Mater.*, 2013, **25**, 6985–6990.
40 J. A. Lee, M. K. Shin, S. H. Kim, H. U. Cho, G. M. Spinks, G. G. Wallace, M. D. Lima, X. Lepro, M. E. Kozlov, R. H. Baughman and S. J. Kim, *Nat. Commun.*, 2013, **4,** 1970.
41 P. L. Taberna, P. Simon and J. F. Fauvarque, *J. Electrochem. Soc.,* 2003, **150**, A292.
42 X. W. Yang, J. W. Zhu, L. Qiu and D. Li, *Adv. Mater.*, 2011, **23**, 2833–2838.
43 F. Huang and D. Chen, *Energy Environ. Sci.*, 2012, **5**, 5833–5841.
44 Q. Q. Zhou, J. Gao, C. Li, J. Chen and G. Q. Shi, *J. Mater. Chem. A*, 2013, **1**, 9196–9201.
45 L. Wang, Y. J. Ye, X. P. Lu, Z. B. Wen, Z. Li, H. Q. Hou and Y. H. Song, *Sci. Rep.*, 2013, **3,** 3568.
46 M. D. Stoller and R. S. Ruoff, *Energy Environ. Sci.*, 2010, **3**, 1294–1301.
47 M. Hughes, M. S. P. Shaffer, A. C. Renouf, C. Singh, G. Z. Chen, J. Fray and A. H. Windle, *Adv. Mater.*, 2002, **14**, 382–385.
48 H. P. Cong, X. C. Ren, P. Wang and S. H. Yu, *Energy Environ. Sci.*, 2013, **6**, 1185-1191.

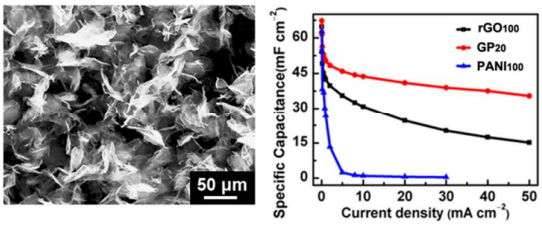

Three-dimensional porous composites of reduced graphene oxide and polyaniline prepared by electro-codeposition exhibited much larger areal specific capacitances, greatly improved rate capability compared with those of their individual components.